Numerical Reconstruction of Ejector Rocket Experimental Tests

A. Matesanz* and A. Velazquez
SENER Ingeniería y Sistemas S.A., 28760 Madrid, Spain
and
J. Tizon‡ and J. Montanes
Universidad Politécnica de Madrid, 28003 Madrid, Spain

Air ejector rocket systems, typical of combined cycle engines for space propulsion applications, have been studied within the ESA Future European Space Transportation Investigations Program. The description and validation of the computational fluid dynamics (CFD) algorithm that has been tuned to simulate the behavior of these systems, and the numerical rebuilding of the ejector rocket experimental tests that were carried out at TNO in The Netherlands are given. The computational developments being presented target the problem of turbulent mixing layer simulation, which is one of the leading phenomena that govern flow behavior inside an ejector rocket. Comparison between experimental and CFD data is given for two validation test cases: a two-dimensional turbulent mixing layer and an axysimmetric ejector in cold flow. Then, the numerical rebuilding of the ejector rocket experimental tests is presented, and the results are discussed with regard to the comparison between numerical and experimental data.

Nomenclature

a = local speed of sound
e = total energy
k = turbulent kinetic energy
M_t = convective Mach number
S = source term
u = velocity along x axis
v = velocity along y axis
w = velocity along z axis
ε = turbulent dissipation
ε_d = dilatation dissipation
ε_s = solenoidal dissipation
μ = viscosity
ρ = density
τ = turbulent stress tensor
τ' = stress tensor

I. Introduction

CONVERGENT–DIVERGENT conical nozzles for propulsion applications have important thrust losses whenever exit pressure is lower than ambient pressure. In this regime, which is normally present in the early stages of flight, losses should be minimized to increase mission effectiveness. This optimization goal could be addressed, for instance, by using ejector nozzles that are characterized by their potential capability to provide thrust augmentation for vertical and short takeoff and landing aircraft, to power supersonic civil aircraft, and to be an alternative to plug nozzles. However, achievement of that goal depends on the capability to carry out, in an efficient way, several complex processes inside the ejector such as ingestion of ambient air, rapid thermal and kinetic mixing, and discharge of the mixture to ambient pressure.

Early theoretical work in ejector rocket analysis and design began by implementing simplifying assumptions such as perfect gas, negligible skin-friction and blockage losses, adiabatic surfaces, complete mixing, etc. In parallel, extensive databases were generated by experimental testing. Furthermore, these experimental data have been generalized in the fashion of generic empirical correlations that collect the available information, and allow for their use as prediction tools. More recently, computational fluid dynamics (CFD) techniques are being applied to the study of ejector nozzle concepts due to their flexibility and capability to deal with complex models.

In the context of ejector rocket performance analysis, Schetz[1] published in 1969 one of the earliest analytical studies on the subject including turbulence models. Some years later, Schetz[2] provided a comprehensive review of theoretical and experimental results that could be used to validate numerical algorithms, among other applications. Optimization and parametric studies have been published by Dutton et al.,[3] Dutton and Carrol,[4] Wacholder and Dayan,[5] Alperim and Wu,[6,7] and Emmanuel.[8] Steffen et al.[9] have provided a computational analysis of an ejector rocket in the rocket-only operation. They concentrated on performance analysis and were able to generalize the results by using statistical design of experiments techniques. After their generalization, they reported that it is possible to make accurate predictions in a six-dimensional design space without having to run additional CFD simulations. Other studies on rocket combined cycles have been published by Granji et al.[10] and Qi et al.[11] Recently, Daines and Segal[12] published an extensive review on rocket-airbreathing combined-cycle systems for space launch applications. The authors reviewed the different technology aspects that characterize this type of propulsion systems and, in particular, they pointed out the synergistic advantages that could be obtained by integrating rocket and airbreathing systems.

One of the most critical aspects to be reckoned with when dealing with numerical computing of ejector rocket aerodynamics behavior is mixing layer modeling and simulation. In fact, successful resolution of this flow structure in complex geometries is a very challenging task from the CFD point of view. With regard to ejector rocket related flow, Bogdanoff,[13] Papamoschou and Roshko,[14] and Papamoschou[15] pointed out that compressibility effects associated to supersonic mixing layers could be described as a function of the convective Mach number M_c. This dimensionless number measures

how far the difference between the speed of the two layers is from the average sound speed.

Very recently, Barber et al.[16] have provided a very interesting paper dealing with the study of the parameters that affect the accuracy of mixing layer prediction. The authors compared the results of five different CFD codes vs two sets of experimental data: a heated supersonic round jet (very relevant for the issue of ejector rocket simulation) and a two-dimensional supersonic mixing layer. In the case of the supersonic round jet, all five codes provided similar outputs; however, the comparison with the experimental results was not very satisfactory. On the other hand, the simulation of the two-dimensional mixing layer proved to be far more accurate. Implementation of several corrections in the algorithms led to an improvement on the prediction of the round jet flow. However, Barber et al. discourage this option because of its inherent lack of generality. Also, they suggest the need to implement a small forward flight component (Mach of the order of 0.05) to strengthen computational stability and to use wall integration instead of wall functions.

In summary, it could be said that incompressible mixing layers are, in general, well understood. Mechanisms controlling growth of the mixing layer as well the mixing process itself are identified and could be modeled after different formulations having several levels of complexity. Compressible and chemically reacting mixing layers, however, are still being subjected to very detailed investigations. The role played by coherent structures, evolution of turbulent flow variables, and influence of compressibility effects are some of the open questions that are now being studied. For the practical design of ejector rocket systems, which rely on accurate prediction of these flow features, models based on semiempirical closures are available, and they could be used confidently for preliminary design purposes. Analysis methods based on k–ε models show a satisfactory combination of accuracy and computational cost, provided that detailed prediction of complex local flow phenomena is not sought. Second-order methods provide a good description of the flowfield, but their associated computational effort, both in terms of time and numerical robustness, is such that they have not reached yet the engineering design departments.

The work presented hereafter addresses the process of numerical rebuilding of the ejector rocket experimental tests that have been carried out in the frame of the ESA Future European Space Transportation Investigations Program (FESTIP). First, the description of the numerical code being used is addressed. Then, validation results are presented, numerical reconstruction of experiments is shown, and conclusions are given.

II. Flow Solver Description

The solver that has been used in this work is of the finite element type. Details concerning its numerical scheme and validation campaign in problems other than ejector rocket related have been published elsewhere by the authors.[17,18] The algorithm uses an explicit time-marching finite element scheme, and the increments of the variables are calculated at each time iteration by using the weak formulation of Navier–Stokes equations. (An integral formulation is used at each element instead of solving a differential equation.[19]) Local time stepping has been implemented to accelerate convergence. Space discretization is performed by means of bilinear quadrangles, and integrals are performed by reduced integration in every element. The stability of the algorithm is enhanced by addition of the following dumping terms: Lapidus artificial diffusivity, fourth-order dissipation term, implicit residual smoothing, and second-order dissipation term activated by a pressure switch. For turbulence modeling, a k–ε formulation has been implemented. Because the k–ε model has a structure that closely resembles that of the Navier–Stokes equations, the same finite element numerical scheme is used to solve both sets of equations. Therefore, upwind and smoothing terms are also applied to the k–ε variables. The law of the wall is applied to the wall boundary conditions.

The standard k–ε model fails to predict the observed decrease in compressible mixing layer spreading rate with increasing Mach number. In this regard, Sarkar et al.[20] and Zeman[21] have proposed models for the ε equation that correct that deficiency. Building on these formulations, Wilcox[22] has postulated a model that is well suited for wall-bounded flow analysis. In these models, the compressible dissipation rate is written in terms of the fluctuating velocity and its divergence:

$$\rho\varepsilon = \rho\varepsilon_s + \rho\varepsilon_d \tag{1}$$

where ε_s and ε_d are the solenoidal and dilatation dissipation that are uncorrelated for high Reynolds number. Obviously, the latter contribution appears only for compressible flows. Sarkar et al.[20] and Zeman[21] postulate that the dilatation component of dissipation should be a function of turbulence Mach number M_t, defined as

$$M_t^2 = 2k/a^2 \tag{2}$$

they argue that the sink terms in the k and ε_s equations should be replaced by

$$\rho\frac{\mathrm{d}k}{\mathrm{d}t} = -\rho(\varepsilon_s + \varepsilon_d) + \cdots, \qquad \rho\frac{\mathrm{d}\varepsilon_s}{\mathrm{d}t} = -\frac{C_{\varepsilon 2}\rho\varepsilon_s^2}{k} + \cdots \tag{3}$$

where $C_{\varepsilon 2}$ is a closure coefficient. Note that both Sarkar et al.[20] and Zeman[21] postulate that equation for ε_s is unaffected by compressibility. To close this model, the dilatation component of dissipation rate is assumed to be proportional to ε_s as follows:

$$\varepsilon_d = \xi^* F(M_t)\varepsilon_s \tag{4}$$

where ξ^* is a closure coefficient and $F(M_t)$ is a prescribed function of M_t. The Sarkar et al.,[20] Zeman,[21] and Wilcox[22] formulations differ in the value of ξ^* and in the functional form of $F(M_t)$. In the work presented in this paper, the Wilcox[22] model has been used. In particular, the model is characterized by the following formulation:

$$\xi^* = \tfrac{3}{2}, \qquad M_{t0} = \tfrac{1}{4} \tag{5}$$

$$F(M_t) = \left(M_t^2 - M_{t0}^2\right)H(M_t - M_{t0}) \tag{6}$$

where $H(x)$ is the Heaviside step function.

Now, nondimensional flow equations (subscript s is dropped as usual practice) in flux vector form are written as

$$\frac{\partial \boldsymbol{Q}}{\partial t} + \frac{\partial \boldsymbol{E}}{\partial x} + \frac{\partial \boldsymbol{F}}{\partial y} + \frac{\partial \boldsymbol{G}}{\partial z} = \frac{\partial \boldsymbol{E}_v}{\partial x} + \frac{\partial \boldsymbol{F}_v}{\partial y} + \frac{\partial \boldsymbol{G}_v}{\partial z} + \boldsymbol{S} \tag{7}$$

where these vectors are defined as follows:

$$\boldsymbol{Q} = \begin{bmatrix} \rho \\ \rho u \\ \rho v \\ \rho w \\ \rho e \\ \rho k \\ \rho\varepsilon \end{bmatrix}, \qquad \boldsymbol{S} = \begin{bmatrix} 0 \\ 0 \\ 0 \\ 0 \\ 0 \\ S_k \\ S_\varepsilon \end{bmatrix} \tag{8}$$

$$\boldsymbol{E} = \begin{bmatrix} \rho u \\ \rho u^2 + p \\ \rho uv \\ \rho uw \\ (\rho e + p)u \\ \rho ku \\ \rho\varepsilon u \end{bmatrix}, \qquad \boldsymbol{E}_v = \begin{bmatrix} 0 \\ \tau'_{xx} \\ \tau'_{xy} \\ \tau'_{xz} \\ u\tau'_{xx} + v\tau'_{xy} + w\tau'_{xz} - q'_x \\ \mu_k \partial k/\partial x \\ \mu_\varepsilon \partial\varepsilon/\partial x \end{bmatrix} \tag{9}$$

$$\boldsymbol{F} = \begin{bmatrix} \rho v \\ \rho uv \\ \rho v^2 + p \\ \rho vw \\ (\rho e + p)v \\ \rho kv \\ \rho\varepsilon v \end{bmatrix}, \qquad \boldsymbol{F}_v = \begin{bmatrix} 0 \\ \tau'_{yx} \\ \tau'_{yy} \\ \tau'_{yz} \\ u\tau'_{yx} + v\tau'_{yy} + w\tau'_{yz} - q'_y \\ \mu_k \partial k/\partial y \\ \mu_\varepsilon \partial\varepsilon/\partial y \end{bmatrix} \tag{10}$$

$$G = \begin{bmatrix} \rho w \\ \rho uw \\ \rho vw \\ \rho w^2 + p \\ (\rho e + p)w \\ \rho kw \\ \rho \varepsilon w \end{bmatrix}, \qquad G_v = \begin{bmatrix} 0 \\ \tau'_{zx} \\ \tau'_{zy} \\ \tau'_{zz} \\ u\tau'_{zx} + v\tau'_{zy} + w\tau'_{zz} - q'_z \\ \mu_k \partial k/\partial z \\ \mu_\varepsilon \partial \varepsilon/\partial z \end{bmatrix} \tag{11}$$

where u, v, w, p, and e are velocity components, pressure, and total energy. Here τ'_{ij} are the terms in the stress tensor, and the q'_i include the effects of heat transfer due to molecular viscosity and turbulence. Also,

$$\mu_k = \mu + \mu_t/\sigma_k \tag{12}$$

$$\mu_\varepsilon = \mu + \mu_t/\sigma_\varepsilon \tag{13}$$

where

$$\mu_t = \rho C_{\mu l}(k^2/\varepsilon) \tag{14}$$

and $C_{\mu l} = 0.081$, $\sigma_k = 1$, and $\sigma_\varepsilon = 1.44$.

The source terms are

$$S_k = \rho P - \rho(\varepsilon + \varepsilon_d) \tag{15}$$

$$S_\varepsilon = \rho C_{\varepsilon 1}(\varepsilon/k)P - f\rho C_{\varepsilon 2}(\varepsilon^2/k) \tag{16}$$

where $C_{\varepsilon 1} = 1.44$, $C_{\varepsilon 2} = 1.83$, and

$$P = \tau_{ij}\frac{\partial u_i}{\partial x_j}, \qquad f = \left[1 - \exp\left(-\frac{y^+}{5.5}\right)\right]^2, \qquad y^+ = \frac{\rho y u_\tau}{\mu} \tag{17}$$

The turbulent stress tensor τ_{ij} is made up by the terms originated by molecular viscosity and turbulent stresses as follows:

$$\rho\tau_{ij} = \tfrac{2}{3}\rho k\delta_{ij} - 2\mu_t\left[\left(S_{ij} - \tfrac{2}{3}S_{kk}\delta_{ij}\right)\right] \tag{18}$$

where

$$S_{ij} = \frac{1}{2}\left(\frac{\partial u_i}{\partial x_j} + \frac{\partial u_j}{\partial x_i}\right) \tag{19}$$

The two-dimensional version of the solver has been used for validation case 1, whereas the axysimmetric version has been used for both validation case 2 and numerical reconstruction of ejector rocket tests.

III. Validation Test Cases

The validation campaign has been carried out at two different levels of complexity. The first one dealt with a two-dimensional compressible shear layer, whereas the second addressed the more realistic geometry of a sonic ejector, whose numerical and experimental results are available in the open literature.

Validation Case 1

The growth rate of a two-dimensional compressible mixing layer has been computed as a function of the convective Mach number M_c. Reynolds number was 3×10^4 based on the mean velocity and initial thickness δ_0 of the mixing layer. The shape of the computational domain was rectangular, and it was made up of 101×201 elements. The experimental data used for comparison have been published by Kline et al.[23] and were reported and also used for validation purposes by Wilcox.[24] Figure 1 shows the computational domain, as well as the comparison between the experimental and numerical growth rate C_δ of the mixing layer as a function of the convective Mach number. This growth rate is defined as

$$\frac{d\delta}{dx} = C_\delta \frac{U_2 - U_1}{U_2 + U_1} \tag{20}$$

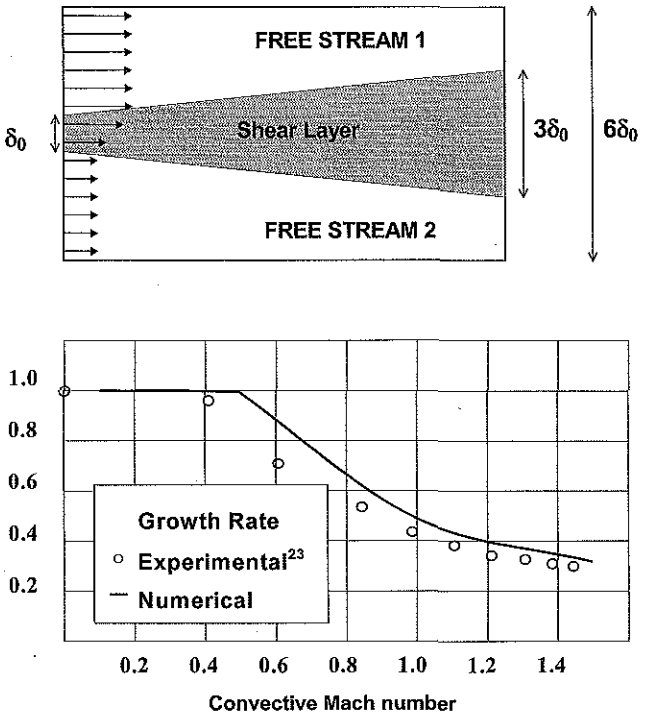

Fig. 1 Two-dimensional Compressible mixing layer: a) overview of the computational domain and b) comparison between experimental[23] and numerical data.

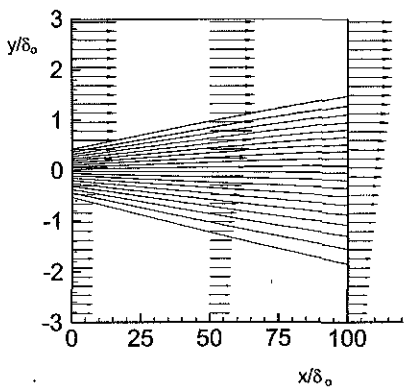

Fig. 2 Velocity profiles across the shear two-dimensional layer.

where δ is the mixing layer thickness and U_1 and U_2 are the velocities at the two freestreams. The maximum deviation between experimental and numerical results occurs at $M_c = 0.6$ and is of the order of 26%. The results improve for higher values of the convective Mach number, and typical errors for $M_c > 1$ are of the order of 10%. Static temperature isoplots that are straight lines with superimposed velocity profiles at three different positions of the computational domain are shown in Fig. 2 for the case $M_c = 0.8$.

Validation Case 2

This second validation case corresponds to an ejector nozzle tested by Gilbert and Hill.[25] The ejector was a simplification of the mixer-ejector nozzles considered in the High-Speed Research Program of NASA. Operating conditions were as follows: Primary rocket nozzle total pressure and temperature were 246 kPa and 358 K, and ambient pressure and temperature were 101 kPa and 395 K, respectively. Rocket exit diameter and duct exit diameter were 0.30 and 4.75 cm, respectively. Figure 3 shows a generic computational domain used for calculations in the vicinity of the primary nozzle and secondary flow inlet. An overview of the Mach number contours is provided in Fig. 3. Positions used to extract radial velocity profiles with the aim of comparing with experimental data are also presented in Fig. 3.

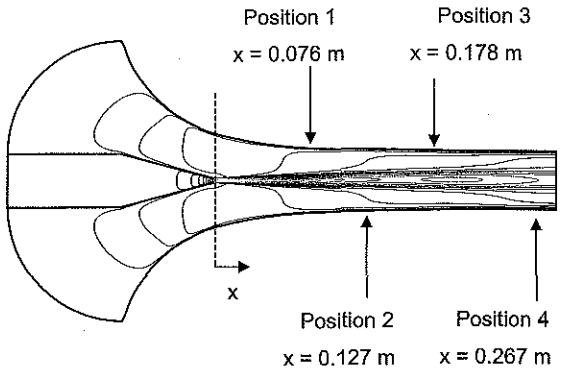

Fig. 3 Overview of the NASA ejector with isomach number contours and positions (1–4) used to extract velocity profiles used for comparison.

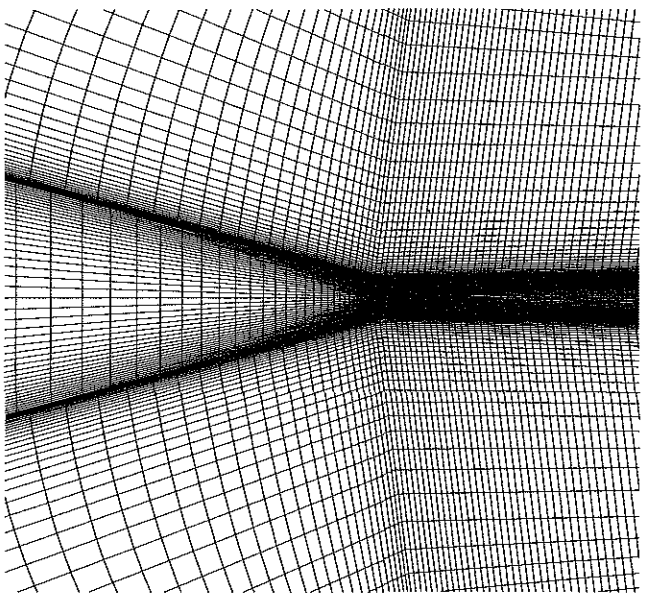

Fig. 4 Closeup of the mesh in the region where primary and secondary flows converge.

The computational domain had 217 horizontal and 83 vertical elements in the upper-half of the ejector. This number of elements was selected after performing a grid independence analysis of the computed solution. Grid topology was adapted to fit the growth of the mixing layer. Also, a similar adaptation was carried out to account for the boundary-layer growth on the outside of the rocket nozzle and on the inside of the diffuser. The x axis was a symmetry line, and positions in the mixing section were measured from the rocket nozzle exit plane (primary flow). An overview of mesh in the vicinity of the rocket exit plane is presented in Fig. 4.

Figures 5 and 6 show the velocity profiles at the four different positions specified in Fig. 2. Experimental data were obtained by Gilbert and Hill.[25] In addition, the numerical results computed by Georgiadis and Yoder[26] when using the Chien[27] turbulence model are included. For each axial station X, the velocity profiles are plotted vs normalized vertical position Y/H, where H is the local distance from the centerline to either the top or bottom wall. These velocity profiles show that the numerical method that has been implemented provides the same level of approximation than the model used by Georgiadis and Yoder.[26] In particular, the spread rate of the mixing layer is simulated satisfactorily, although mixing close to the nozzle exit is somewhat underpredicted. The agreement with experimental data tends to improve downstream of the nozzle exit.

One of the most critical aspects to be solved during the numerical convergence process was secondary flow acceleration from the entrance of the computational domain (Mach number close to 0) to the rocket nozzle exit plane (primary flow). Boundary conditions that were used at the entrance of the secondary flow computational

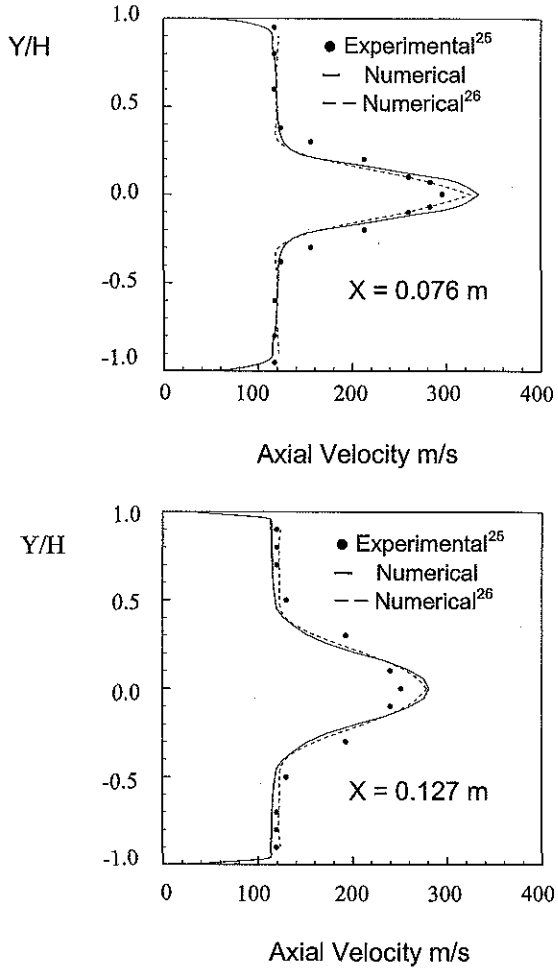

Fig. 5 Flow profiles inside the NASA ejector at stations 0.076 and 0.127 m: ●, experimental data of Gilbert and Gill[25]; ——, numerical simulation; and – – –, numerical results of Georgiadis and Yoder.[26]

domain were total pressure equal to ambient pressure and total temperature equal to ambient temperature. Because of the subsonic character of the flow in that region, no additional boundary condition on the velocity normal to the computational domain entrance section was needed. Figure 7b shows Mach number evolution (from 0.04 to 0.2) along the three straight lines that are given in Fig. 7a. Observe that the flow is smoothly accelerated so that it reaches the rocket nozzle exit without major disturbances.

IV. Numerical Reconstruction of FESTIP Experiments

An extensive ejector rocket flow experimental campaign was conducted within the ESA FESTIP at TNO in The Netherlands by Dijkstra et al.[28] The objective of the campaign was to investigate ejector rocket performance under a variety of conditions. An axysimmetric ejector rocket was considered that entrained ambient air from the test room. Rocket flow was supersonic, whereas the entrained air had to accelerate down from rest conditions up to the appropriate velocity in the mixing duct. The geometry that was considered is presented in Fig. 8. The ejector itself had a length of 0.954 m, and it was followed by a shorter (0.252 m) slightly divergent diffuser. In some of the test cases, a small constriction was placed at the end of the ejector (Fig. 8). An expanded view of the rocket region is presented in Fig. 9. Two different nozzles were used for the rocket whose operating and geometrical parameters are given in Table 1.

In regard to the numerical reconstruction activity, multiblock structured grids, refined near the boundary and mixing layers regions, were used. A grid independence analysis was performed, and it showed that no further improvements were obtained on the solution for grids having more than 30,000 points. When looking at the lower limit of mesh size, differences in computed thrust and bypass

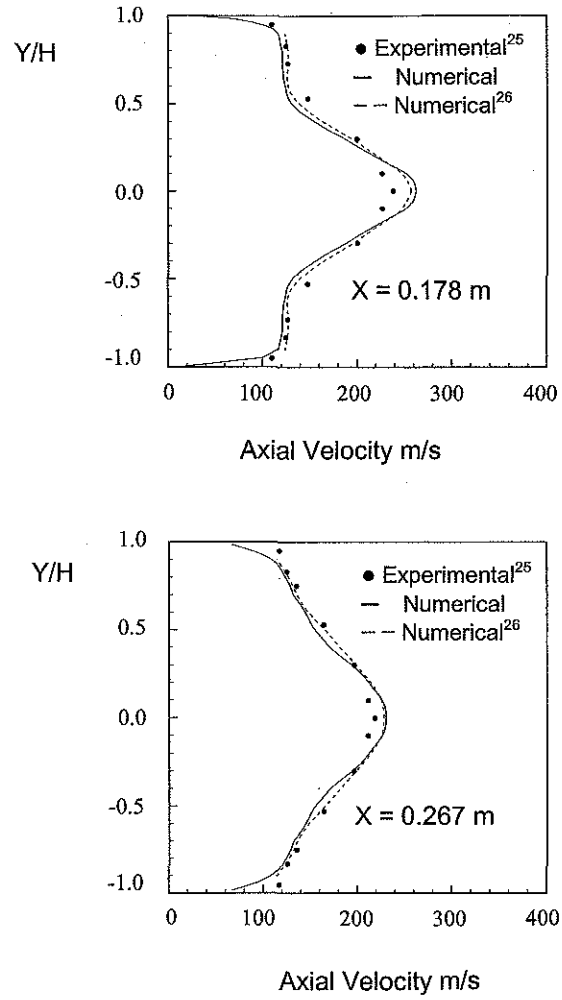

Fig. 6 Flow profiles inside the NASA ejector at stations 0.178 and 0.267 m: ●, experimental data of Gilbert and Gill[25]; ——, numerical simulation; and – – –, numerical results of Georgiadis and Yoder.[26]

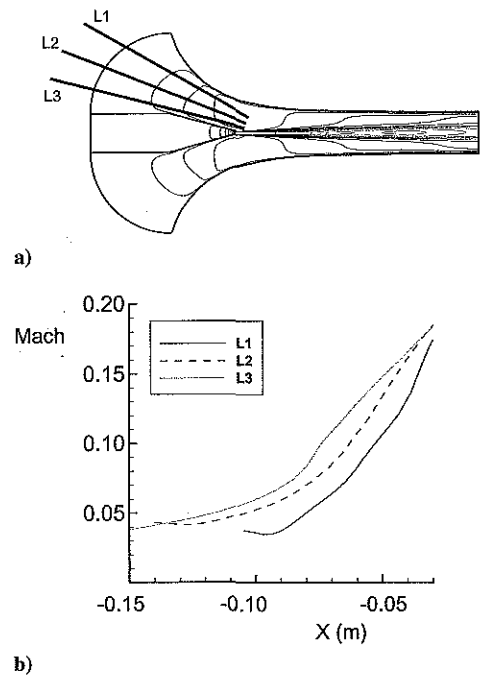

Fig. 7 Mach number profiles along three different straight lines inside the acceleration region of the secondary flow.

Table 1 Geometrical and operational parameters of the two rockets used in the experimental tests

Parameter	Rocket 1	Rocket 2
Throat diameter, m	0.016	0.0225
Area ratio	4	4
Total temperature, K	2440	2440
Total pressure, MPa	1, 2, 3	1, 2, 3
Exit static temperature, K	1310	1310
Exit static pressure, MPa	0.12	0.12
Exit Mach number	2.7	2.7
Reynolds number	2×10^6	2×10^6

Table 2 Definition of experimental tests cases

Case number	Rocket chamber pressure, MPa	Rocket nozzle throat diameter, m	Constriction present
1	1	0.016	No
2	1	0.016	Yes
3	2	0.016	No
4	2	0.016	Yes
5	3	0.016	No
6	3	0.016	Yes
7	1	0.0225	No
8	1	0.0225	Yes
9	2	0.0225	No
10	2	0.0225	Yes
11	3	0.0225	No
12	3	0.0225	Yes

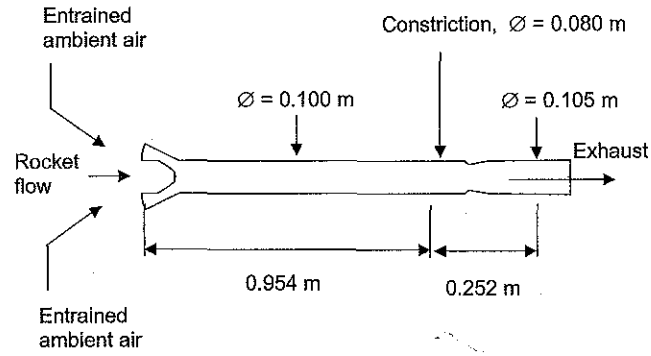

Fig. 8 Overview of the TNO ejector rocket.

ratio were less than 4% for meshes having 10,000 and 30,000 points, respectively. Figure 10 shows a closeup view of the 30,000 points mesh in the vicinity of the rocket nozzle exit. As in validation case 2, the mesh was adapted to fit mixing layer growth.

Instead of looking at the numerical residuals, the numerical process was considered as converged when the time derivative of the bypass ratio was lower than a predetermined value. In general, it could be said that convergence processes were long and difficult. The cases with the lower exit rocket pressure, that had the slower bypass ratio evolution, needed on the order of 500,000 iterations to reach the prescribed convergence criterion. The computational time was $8.1e{-}6$ seconds per point per iteration in a 1-GHz Intel-based Pentium personal computer. Table 2 presents the definition of the 12 test cases that have been simulated.

One of the aspects that had to be reckoned with during the simulation process was the selection of the specific heats ratio γ of the mixture. Basically, the ambient air was a perfect gas with constant γ (equal to 1.4), whereas rocket flow could also be modeled as perfect gas having a different γ (equal to 1.237). That is, we had to deal with the mixture of two perfect gases having different values of γ, and, therefore, the problem was the selection of an effective γ for each of the grid points where the numerical solution was sought. We considered that an appropriate index of the mixing extent at any given grid point was the total temperature at that point. The reason was that each of the two perfect gases was characterized by

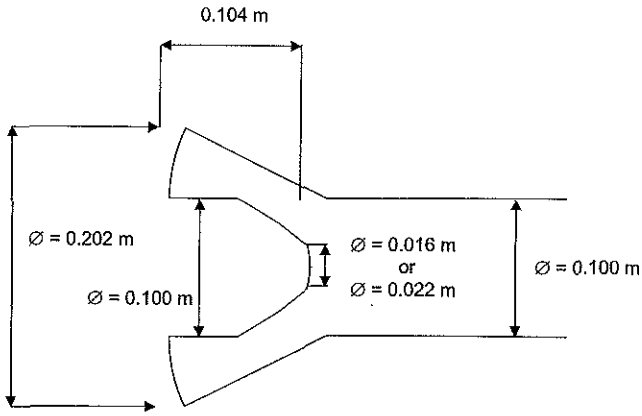

Fig. 9 Closeup of the TNO ejector rocket in the region where primary and secondary flows converge.

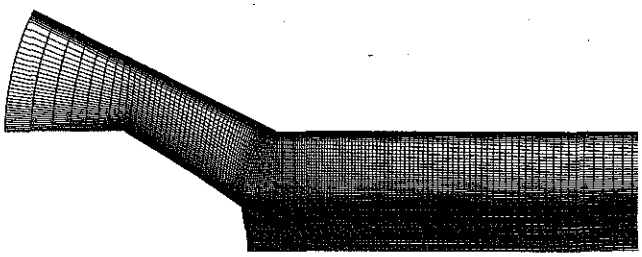

Fig. 10 Closeup of the mesh used for computations in the region where primary and secondary flows converge.

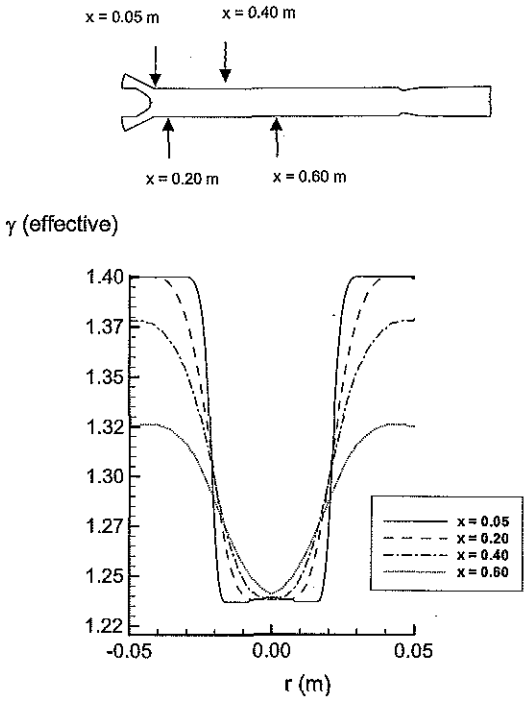

Fig. 11 Effective γ profiles at four different positions inside the ejector.

a different total temperature, and one the of effects of the mixing process (that depends on static temperature and velocity) was to change total temperature. Accordingly, we worked out a relation between effective gamma and total temperature by using the mass fraction of each gas as the connecting parameter. Once this relation was built up, it was implemented as a subroutine in our numerical simulation algorithm. Profiles of the effective γ downstream of the rocket nozzle exit at different locations are plotted in Fig. 11 for test case number 6 (Table 2). With regard to the C_p, the gas generator

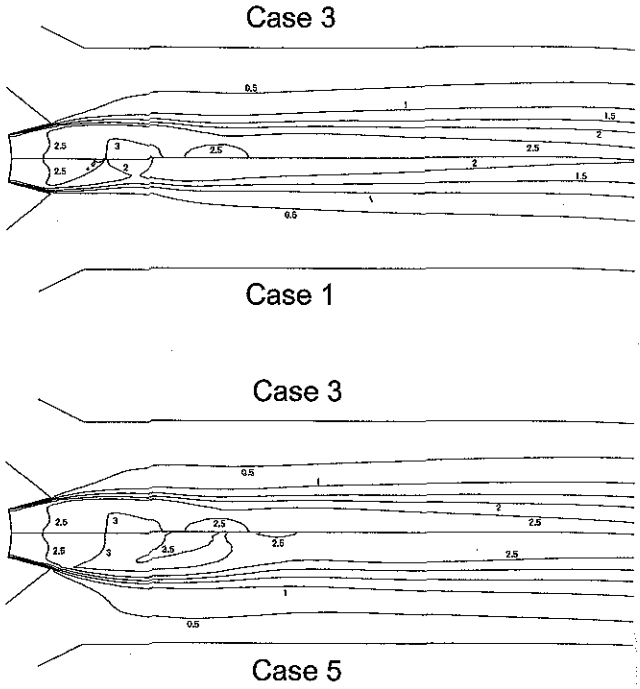

Fig. 12 Isomach lines for cases 1, 3, and 5: case 3 upper half and cases 1 and 5 lower half.

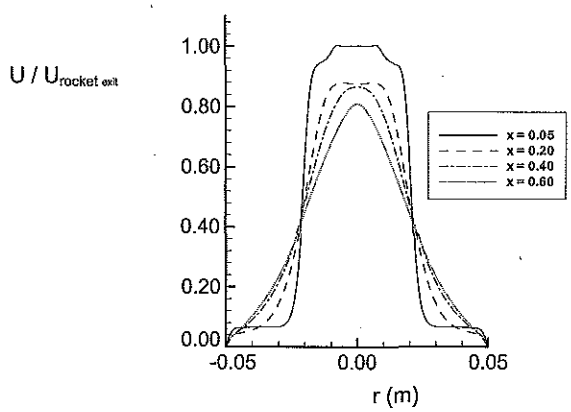

Fig. 13 Dimensionless axial velocity at four different positions inside the ejector.

that fed the rocket was operated with a mixture of ethane (C_2H_4) and air as oxidizer. The mixture was very oxidizer rich, and this allowed us to take the C_p of the rocket gases as 287 J/kg · K.

Figure 12 shows isomach lines in the region close to the rocket nozzle exit for test cases 1, 3, and 5 (Table 2). Outgoing rocket flow in case 3 was nearly adapted, and this is why it is compared with cases 1 (overexpanded) and 5 (underexpanded). Observe that the topology of the local flow structure at the rocket nozzle exit had an influence on the downstream mixing characteristics: Higher rocket exit pressure caused more efficient mixing and entrainment. This is consistent with that higher rocket exit pressure means that the supersonic flow region downstream of the exit section (see lower half of Fig. 12) is also larger. Then, this large energy region has a large capability to entrain ambient air. An indication of how fast the mixing process proceeds could be gathered from the smoothing of the flow velocity profiles inside the ejector. Figure 13 shows dimensionless velocity profiles at the locations specified in Fig. 11.

Figure 14 presents the comparison between measured and computed wall static pressure along the mixer axial coordinate in the cases with the smallest rocket nozzle throat diameter (test cases 1–6). In these cases, maximum deviation between experimental and numerical data was of the order of 15%. In cases 7–12,

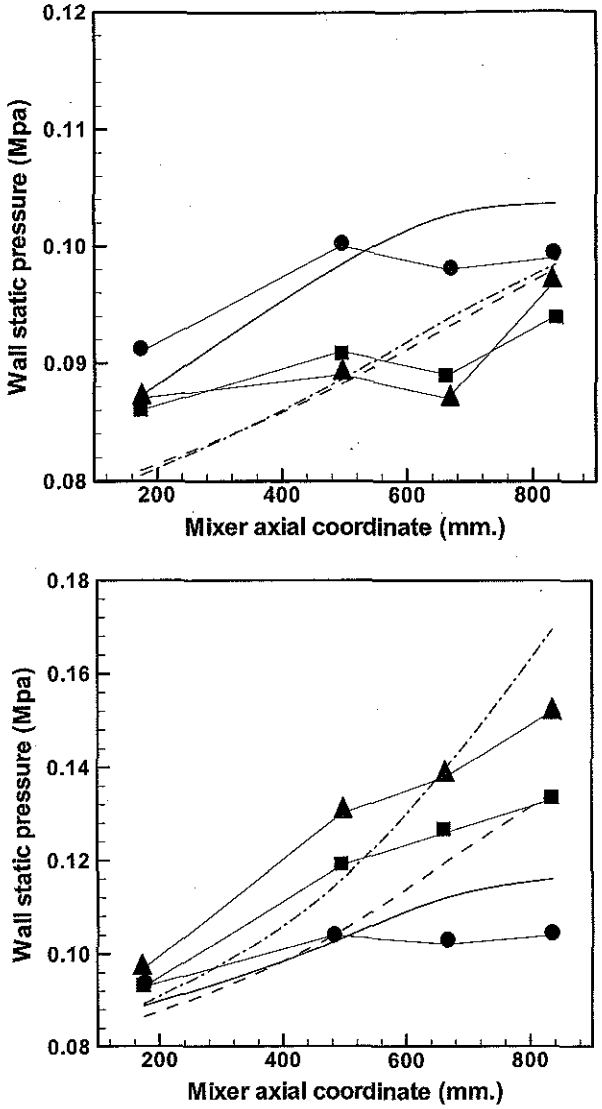

Fig. 14 *Comparison between experimental*[28] *and computed static* pressures along the ejector wall for different cases: a) ●, case 1 experimental; ——, case 1 numerical; ■, case 3 experimental; – – –, case 3 numerical; ▲, case 5 experimental; and –·–, case 5 numerical and b) ●, case 2 experimental; ——, case 2 numerical; ■, case 4 experimental; – – –, case 4 numerical; ▲, case 6 experimental; and –·–, case 6 numerical.

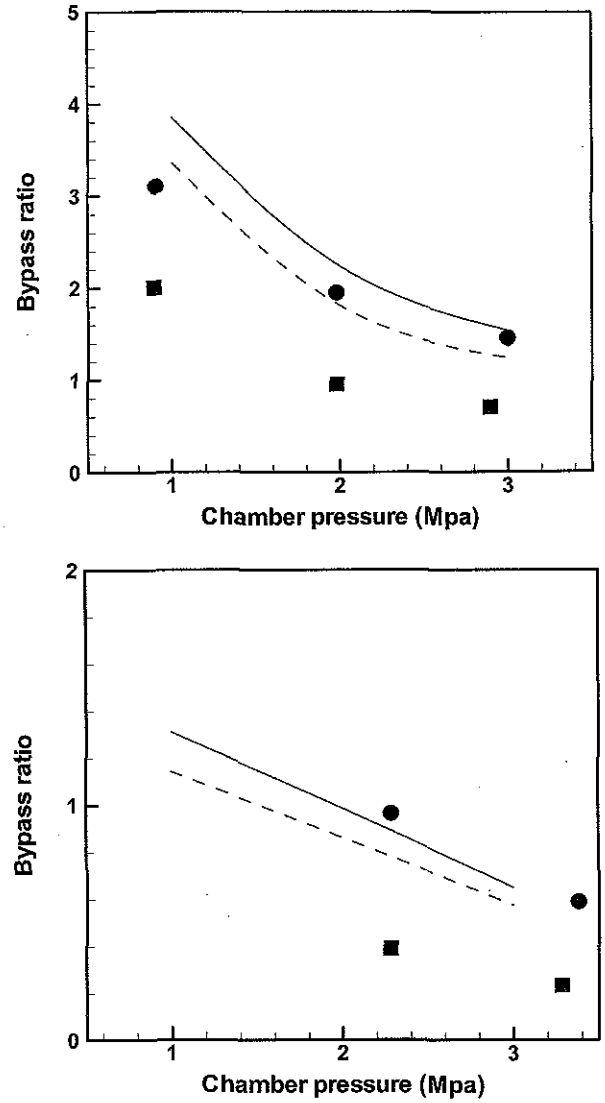

Fig. 15 Comparison between experimental[28] and computed bypass ratios as a function of the rocket chamber pressure: a) ●, experimental cases 1, 3, and 5; ——, numerical cases 1, 3, and 5; ■, experimental cases 2, 4, and 6; and –·–, numerical cases 2, 4, and 6 and b) ●, experimental cases 9 and 11; ——, numerical cases 7, 9, and 11; ■, experimental cases 10 and 12; and –·–, numerical cases 8, 10, and 12.

maximum deviation between measured and computed data was of the order of 20%. Test cases that did not have the constriction at the end of the mixer proved to be far easier to converge, and in this situation, differences between CFD and experiments were always less than 8%.

When the bypass ratio is examined (defined as the ratio between entrained air and rocket mass flow) accuracy of the prediction appeared to deteriorate (Fig. 15). In cases without constriction, differences between experimental and numerical simulation data peaked at a maximum of 25%, whereas these differences climbed up to 70% in the cases with constriction. However, the question of the accuracy of measurements needs to be accounted for at this stage. In particular, the authors of the experimental campaign[28] reported that the entrained mass flow was measured by using a single pitot-static tube at the mixer entrance and that corrections were implemented to account for the influence of velocity profiles. This means that the experimentally measured bypass ratio has to be regarded as merely indicative of the physical trend.

In our view, it appears that the present level of modeling does not suffice to make really accurate predictions of the entrained mass flow. A somewhat similar conclusion was drawn by Dijkstra et al.[28] when they used a quasi-one-dimensional model to predict the flow variables of interest in their experiments. In their case, they ascribed the discrepancies to three possible causes: errors in the experimental measurements, losses due to unaccounted friction and three-dimensional effects, and variations in the rocket exit conditions. In our case, we tend to agree with the conclusions of Barber et al.[16] that point in the direction of the deficiencies in the turbulence models used for compressible shear layer simulation. These authors,[16] who carried out an extensive comparison between five different flow solvers, reported poor agreement when dealing with the prediction of mixing of round jets and found that their results were strongly dependent on the turbulence model being used. In our paper, we have used a finite element algorithm and a k–ε turbulence model with the Wilcox[22] correction for compressibility effects. Barber et al.[16] used finite volume based algorithms together with k–ε turbulence models implementing the Sarkar et al.[20] and Zeman[21] corrections. However, in both cases the results were not satisfactory with regard to the prediction of mixing phenomena. For instance, that numerical solutions promote mixing faster than nature does appears to be a common trend in all models under consideration. One of the reasons that could account for this discrepancy might be associated to the large temperature difference between the entrained air and the

rocket flow. In particular, rocket total temperature was as high as 2440 K in our case. Also, the use of an effective gamma interpolated as a function of the total temperature may not be fully adequate, and a more accurate model might be needed. Another aspect that has to be considered is that choking occurs at the configuration without contraction for the higher flow rate cases, and it is always present in the tests carried out with the contraction put in place. This further complicates the numerical resolution of the problem, and we believe that it also contributes to explain the discrepancies observed. Furthermore, from the computational side, it should be said that explicit algorithms, such as the one we use, are not very well suited to analyse flow behavior inside long and narrow computational domains.

V. Conclusions

A finite element Reynolds averaged Navier–Stokes solver has been tuned to deal with the reconstruction of the ejector rocket experimental tests carried out in the frame of the ESA-FESTIP. Validation of the solver was carried out considering two cold flow cases: the growth rate of a planar shear layer and the velocity profiles inside an axisymmetric ejector that was experimentally tested at NASA. In these two cases, the solver produced results that show a reasonable agreement with the experimental data.

With regarding to the numerical reconstruction of the hot flow FESTIP ejector rocket tests, the results obtained showed a mixed performance. Prediction of static pressure all along the ejector rocket wall was fairly accurate for engineering design purposes. Errors were smaller than 10% when no constriction was present in the ejector, whereas discrepancies close to 15% were observed when a constriction was placed at the end of the mixer. However, it was found that the bypass ratio, which measures the entrained air mass flow, was poorly predicted. In fact, the discrepancies between measured and simulated results were as high as 70%. In any case, there remain doubts about the accuracy of the experimental bypass ratio measurements.

Nevertheless, even though it is clear that the measurement system of the experimental setup bears some influence on the discrepancies that were observed, we believe that this might not be the most critical. When the evidence presented by other researchers (Barber et al.[16]) who have dealt with a somewhat similar problem by using different simulation means is examined, we believe that the main reason for the discrepancies could be associated to the modeling of the turbulent shear layer. For instance, that the static temperature at the rocket exit section was 1310 K might account for some of the discrepancies that were not found in the cold flow validation cases. Also, it appears that different corrections for the compressibility effects in the k–ε equations tend to promote numerical mixing that occurs much faster than in nature. It could be concluded that, although existing models for shear layer mixing prediction indeed help the aerospace engineer to simulate complex flows inside rocket-based combined cycles, numerical results should be regarded with caution. That is, these results should be used in a qualitative rather than in a quantitative way for design purposes, and it follows that there is a clear need to keep improving these physical models that have such a relevant influence for aerospace vehicle system analysis. In addition, the existence of choking in the flowfield, as well as the fact that explicit methods are not fully adequate to treat long and narrow computational domains might also be additional reasons for the observed discrepancies.

Acknowledgment

The authors are grateful to F. Dijkstra at TNO for providing the results of the ejector rocket tests.

References

[1]Schetz, J. A., "Unified Analysis of Turbulent Jet Mixing," NASA CR-1382, 1969.

[2]Schetz, J. A., "Injection and Mixing in Turbulent Flow," edited by M. Summerfield, Vol. 68, Progress in Astronautics and Aeronautics, AIAA, Washington, DC, 1980.

[3]Dutton, J. C., Mikkelsen, C. D., and Addy, A. L., "A Theoretical and Experimental Investigation of the Constant Area, Supersonic–Supersonic Ejector," *AIAA Journal*, Vol. 20, No. 10, 1982, pp. 1392–1400.

[4]Dutton, J. C., and Carroll, B., "Optimal Supersonic Ejector Designs," *Journal of Fluids Engineering*, Vol. 108, No. 4, 1986, pp. 414–420.

[5]Wacholder, E., and Dayan, J., "Application of the Adjoint Sensitivity Method to the Analysis of a Supersonic Ejector," *Journal of Fluids Engineering*, Vol. 106, No. 4, 1984, pp. 425–429.

[6]Alperin, M., and Wu, J., "Trust Augmenting Ejectors, Part 1," *AIAA Journal*, Vol. 21, No. 10, 1983, pp. 1428–1436.

[7]Alperin, M., and Wu, J., "Trust Augmenting Ejectors, Part 2," *AIAA Journal*, Vol. 21, No. 10, 1983, pp. 1698–1706.

[8]Emanuel, G., "Optimum Performance for a Single-Stage Gaseous Ejector," *AIAA Journal*, Vol. 14, No. 9, 1976, pp. 1292–1296.

[9]Steffen, C. J., Smith, T. D., Yungster, S., and Keller, D. J., "Computational Analysis for Rocket Based Combined-Cycle Systems During Rocket Only Operation," *Journal of Propulsion and Power*, Vol. 16, No. 6, 2000, pp. 1030–1039.

[10]Ganjji, A. R., Khadem M., and Khandani, S. M., "Turbo Air Augmented Rocket: A Combined-Cycle Propulsion System," *Journal of Propulsion and Power*, Vol. 7, No. 4, 1991, pp. 650–653.

[11]Qi, F., Wang, J., and Chen, C. P., "Preliminary Analysis of an Airbreathing and Rocket Combined-Cycle Engine," *Journal of Propulsion and Power*, Vol. 14, No. 5, 1998, pp. 613–619.

[12]Daines, R., and Segal, C., "Combined Rocket and Airbreathing Propulsion Systems for Space Launch Applications," *Journal of Propulsion and Power*, Vol. 14, No. 5, 1998, pp. 605–612.

[13]Bogdanoff, D. W., "Compressibility Effects in Turbulent Shear Layers," *AIAA Journal*, Vol. 21, No. 6, 1983, pp. 926, 927.

[14]Papamoschou, D., and Roshko, A., "The Compressible Turbulent Shear Layer: An Experimental Study," *Journal of Fluid Mechanics*, Vol. 197, 1988, pp. 453–477.

[15]Papamoschou, D., "Structure of the Compressible Turbulent Shear Layer," *AIAA Journal*, Vol. 29, No. 5, 1990, pp. 680, 681.

[16]Barber, T. J., Chiapetta, L. M., DeBonis, J. R., Georgiadis, N. J., and Yoder, D. A., "Assessment of Parameters Influencing the Prediction of Shear Layer Mixing," *Journal of Propulsion and Power*, Vol. 15, No. 1, 1999, pp. 45–53.

[17]Matesanz, A., Velázquez, A., Jiménez, A., and Rodríguez, M., "Numerically Robust 3-D Finite Element Reynolds Averaged Navier Stokes Solver for the Study of Turbulent Supersonic External Flows," *Computer Methods in Applied Mechanics and Engineering*, Vol. 159, No. 3-4, 1998, pp. 383–394.

[18]Matesanz, A., and Velázquez, A., "EARSM Finite Element Solver for the Study of Turbulent 3-D Compressible Separated Flows," *Computer Methods in Applied Mechanics and Engineering*, Vol. 190, No. 8–10, 2000, pp. 989–1004.

[19]Taylor, C., and Hughes, T. G., "Finite Element Programming of the Navier–Stokes Equations," Pineridge, Swansea, Wales, U.K., 1981.

[20]Sarkar, S., Erlebacher, G., Hussaini, M. Y., and Kreiss, H. O., "The Analysis and Modelling of Dilatational Terms in Compressible Turbulence," ICASE Rept. 89-79, Dec. 1989.

[21]Zeman, O., "Dilatational Dissipation. The Conceptual Application in Modelling Compressible Mixing Layers," *Physics of Fluids A*, Vol. 2, No. 2, 1990, pp. 178–188.

[22]Wilcox, D. C., "Dilatation–Dissipation Corrections for Advanced Turbulence Models," *AIAA Journal*, Vol. 30, No. 11, 1992, pp. 2639–2646.

[23]Kline, S. J., Cantwell, B. J., and Lilley, G. M., "Comparison of Computations and Experiments," edited by Kline, Cantwell and Lilley, AFOSR-HTTM Stanford Conf. on Complex Turbulent Flows, March 1982.

[24]Wilcox, D. C., *Turbulence Modeling for CFD*, edited by DCW Industries, La Cañada, CA, 1994.

[25]Gilbert, G. B., and Hill, P. G., "Analysis and Testing of Two-Dimensional Slot Nozzle Ejectors with Variable Area Mixing Sections," NASA CR-2251, 1973.

[26]Georgiadis, N. I., and Yoder, D. A., "Use of Navier–Stokes Methods for the Calculation of High Speed Nozzle Flow Fields," NASA TM-106551, June 1994.

[27]Chien, K. Y., "Predictions of Channel and Boundary Layer Flows with a Low Reynolds Number Turbulence Model," *AIAA Journal*, Vol. 20, No. 1, 1982, pp. 33–38.

[28]Dijkstra, F., Maree, A., Caporicci, M., and Immich, H., "Experimental Investigation of the Thrust Enhancement Potential of Ejector Rockets," AIAA Paper 97-2756, July 1997.